International Conference on Pattern Recognition
August 2002, I: 532-535

Level Set Evolution with Region Competition: Automatic 3-D Segmentation of Brain Tumors

[1]Sean Ho, [2]Elizabeth Bullitt, and [1,3]Guido Gerig
[1]Department of Computer Science, [2]Department of Surgery, [3]Department of Psychiatry
University of North Carolina, Chapel Hill, NC 27599, USA
email: gerig@cs.unc.edu

Abstract— **This paper discusses the development of a new method for the automatic segmentation of anatomical structures from volumetric medical images. Driving application is the segmentation of 3-D tumor structures from magnetic resonance images (MRI), which is known to be a very challenging segmentation problem due to the variability of tumor geometry and intensity patterns. Level set evolution combining global smoothness with the flexibility of topology changes offers significant advantages over conventional statistical classification followed by mathematical morphology. Level set evolution with constant propagation needs to be initialized either completely inside or outside and can leak through weak or missing boundary parts. Replacing the constant propagation term by a signed local statistical force overcomes these limitations and results in a region competition method that converges to a stable solution.**

Applied to MR images presenting tumors, probabilities for background and tumor regions are calculated from a pre- and post-contrast difference image and mixture-modelling fit of the histogram. The whole image is used for initialization of the level set evolution to segment the blobby-shaped tumor boundaries. Preliminary results on five cases presenting different tumors with significant shape and intensity variability demonstrate that the new method might become a powerful and efficient tool for the clinic. Validity is demonstrated by comparison with manual expert segmentation.

I. Introduction

Segmentation of volumetric image data is still a challenging problem, and successful solutions either are based on simple intensity thresholding or by model-based deformation of templates. The former implies that structures are well separated by unique intensity patterns, whereas the latter requires model templates characteristic for the shape class. Snakes [1] are appealing to users as they only require a coarse initialization but then converge to a stable, fully reproducible boundary. Applications with real imagery, however, demonstrate that "snakes are only as good a their initialization", implying that a user would have to provide an initial solution close to the optimal solution in order to guarantee a successful result. In three dimensional data, this is not a viable option. Snakes based on level set evolution, on the other hand, are appealing especially for volumetric data processing [2], [3], [4]. The formalism can be naturally extended from 2D to higher dimensions, and the resulting zero level sets offer flexible topology. A powerful extension is obtained by combining level set evolution with statistical shape constraints [5], but this is not possible in our driving application of segmenting tumors of variable size and location. Level set evolution with fixed propagation direction is either initialized inside or outside sought objects, and the propagation force is opposed by a strong gradient magnitude at image discontinuities. At locations of missing or fuzzy boundaries, the internal force is often strong enough to counteract global smoothness and leaks through these gaps. Thus, there is no convergence and the evolution has to be halted manually. This observation led to a new concept of region competition, where two adjacent regions compete for the common boundary [6], additionally constrained by a smoothness term.

Supported by NIH-NCI R01 CA67812. Partially supported by NIH-NCI P01 CA47982.

The driving problem discussed in this paper is the segmentation of 3-D brain tumors from magnetic resonance image data. Tumors vary in shape, size, location, and internal texture, and tumor segmentation is therefore known to be a very challenging and difficult problem. Intensity thresholding followed by erosion, connectivity, and dilation is a common procedure but only applicable to a small class of tumors presenting simple shape and homogeneous interior structure. Warfield et al. [7], [8], [9] demonstrated a methodology based on elastic atlas warping for brain extraction and statistical pattern recognition for brain interior structures. The intensity feature was augmented by a "distance from the boundary" feature to account for overlapping probability density functions. As a final step, structures went through opening/closing steps to segment blobby, connected structures. The method has been shown to be successful for simply-shaped tumors with homogeneous texture.

The approach presented herein aims at providing a more generic and fully automatic method for the segmentation of blobby-shaped tumor structures. We developed a 3-D level set method in a region competition framework. Variable topology and smoothness serve as key features to group tumor candiate regions to blobby-shaped, connected 3-D objects. Crucial for potential clinical applications is also the development of a highly efficient and robust method.

II. Tumor Segmentation Procedure

Our tumor segmentation procedure starts with an intensity-based fuzzy classification of voxels into tumor and background classes. The details of this initial classification are given in Section IV-B. This tumor probability map is then used to locally guide the propagation direction and speed of a level-set snake. The tumor probability map is also used to derive an automatic initialization of the snake. Image forces are balanced with global smoothness constraints to converge stably to a smooth blobby tumor segmentation of arbitrary topology.

A. Multiparameter Image Data

Our images are multichannel 3D magnetic resonance images that show different aspects of the tumor region. High-resolution T1-weighted MRIs are commonly used for detailed imaging of neuroanatomy, but by themselves do not distinguish tumor tissue well. T2-weighted MRIs do highlight tumor tissue and surrounding edema, but are often difficult to obtain in high resolution. Of great use is a post-contrast T1-weighted MRI, where contrast agent has been injected into the bloodstream to highlight the tumor. In this work we use T1-weighted pre- and post-contrast 3D images.

B. Image Forces

In a deformable model segmentation scheme, the model is driven by image forces and constrained by prior information on the shape of the model. In classical snakes, the image forces are generally governed by the gradient magnitude, and the shape prior is a form of smoothness. Using the level-set snakes framework, the image forces and smoothness constraints are simply separate terms in the partial differential equation governing the evolution of the implicit function defining the snake.

The traditional "balloon" snakes, with a constant propagation term, have the issue that the propagation term has a fixed sign; i.e. the balloon can only grow or only shrink. Hence the snake must be initialized either completely inside the target object, or completely circumscribing the target object. In our snake model, the propagation term is locally modulated by a signed image force factor between -1 and +1, causing the snake to shrink parts outside the tumor and expand parts inside the tumor. Hence our snake can be initialized partially inside and partially outside the tumor; it is more robust to initialization.

C. Smoothness Constraints

If the snake were only guided by image forces, it would leak into many small noisy structures in the image that are not part of the tumor. A commonly used, standard way to constrain level-set snakes is to apply mean curvature flow to the snake contour; in the level-set formalism this is easily done by adding a term to the snake evolution equation. We also apply a smoothing to the implicit function in order to aid numerical stability of the algorithm.

III. Level Set Snake Evolution

A classical level set snake is defined as the zero level set of an implicit function ϕ defined on the entire image. The evolution of the snake is defined via a partial differential equation on the implicit function ϕ.

Consider a level set snake which propagates normal to its boundary uniformly at a constant speed α:

$$\frac{\partial \phi}{\partial t} = \alpha \left|\nabla \phi\right|$$

Our region competition-based snake modulates this propagation term using image forces to change the direction of propagation, so that the snake shrinks when the boundary encloses parts of the background (B), and grows when the boundary is inside the tumor region (A):

$$\frac{\partial \phi}{\partial t} = \alpha(P(A) - P(B)) \left|\nabla \phi\right|$$

The image forces need to be balanced with some smoothness constraints; a standard technique is to apply mean curvature flow to the snake contour. The strength of the smoothing is controlled with a constant multiplicative factor c_{MCF}:

$$\begin{aligned} \frac{\partial \phi}{\partial t} &= \alpha(P(A) - P(B)) \left|\nabla \phi\right| \\ &+ c_{\mathrm{MCF}} \nabla \cdot \left(\frac{\nabla \phi}{|\nabla \phi|}\right) |\nabla \phi| \end{aligned}$$

Lastly, to help ensure numerical stability of the forward-in-time, centered-in-space (FTCS) solution of the partial differential equation, we apply a uniform smoothing to the implicit function ϕ. An additional constant factor c_{sm} controls the strength of this smoothing:

$$\begin{aligned} \frac{\partial \phi}{\partial t} &= \alpha(P(A) - P(B)) \left|\nabla \phi\right| \\ &+ c_{\mathrm{MCF}} \nabla \cdot \left(\frac{\nabla \phi}{|\nabla \phi|}\right) |\nabla \phi| \\ &+ c_{\mathrm{sm}} \nabla^2 \phi \end{aligned}$$

IV. Application to tumor segmentation

A. MRI methods

Our image datasets are from patients with meningioma and glioblastoma brain tumors, acquired on a 1.5T clinical scanner (except for one acquired on a 3T scanner). T1-weighted and T2-weighted images were acquired of the whole head, as well as T1-weighted images after gadolinium MRI contrast agent was injected into the patient's bloodstream in order to highlight the tumor. The T1-weighted images have an in-plane resolution of 256x256 and about 120 slices (depending on the individual dataset), with a voxel resolution of $1 \times 1 \times 1.5mm^3$.

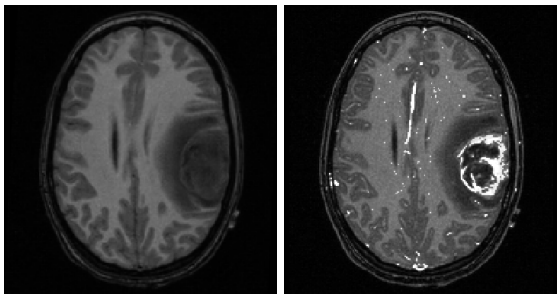

Fig. 1. Axial cross-section of T1-weighted 3D MRI, without (left) and with (right) contrast agent.

B. Tumor probability map

Of critical importance in the formulation of the competition level-set snake is the probability map, a scalar field on the image which specifies, voxel by voxel, a probability

that the given voxel belongs to the tumor or to the background. The two T1-weighted images, with and without contrast agent, are registered using MIRIT [10] and a difference image is obtained voxel-by-voxel. The histogram of this difference image (see Fig. 2) clearly shows a symmetric distribution around zero and a second distribution related to regional changes caused by contrast. The second distribution is asymmetric but strictly on the positive axis, which relates to larger regions accumulating a small amount of contrast and very small regions strongly highlighted by contrast. In this preliminary work, we fit the histogram by a mixture density of two distributions, a Gaussian function to model small differences around zero and a Poisson distribution to model the changes due to contrast. We use the NonlinearFit package provided by Mathematica. The scalar field derived from the posterior probability with range $[-1, 1]$ is passed into the level-set algorithm as the probability map $P(A) - P(B)$ shown in Figure 3(a).

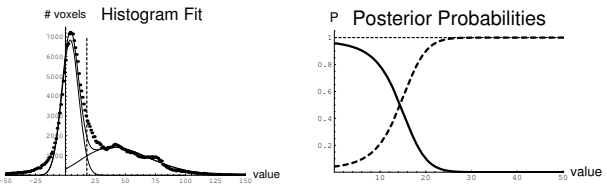

Fig. 2. Histogram of post- and pre-contrast difference image and fit with two distributions (left) and posterior probabilities (right). Differences around zero are fitted with a Gaussian, whereas the contrast uptake is fitted with a Poisson function. The resulting threshold is shown as a dotted vertical line. Posterior probabilities for background (straight) and tumor (dotted) as a function of difference image value are shown in the right figure.

For computational speed, the datasets are subsequently cropped to the region around the tumor, however the algorithm works just as well on the whole brain.

The probability map from the difference image is rather noisy, and includes many regions that should not be considered part of the tumor. It is known that blood vessels and bone marrow also take up gadolinium. In addition, the ring-shaped gadolinium enhancement common in glioblastoma tumors results in misclassification of many voxels in the center of the tumor. It is clear that intensity-based tissue classification alone is insufficient for satisfactory segmentation of the tumor. The level-set snake uses this fuzzy classification heavily for its image forces, but adds needed smoothness constraints. Future work will look at using atlas-based fuzzy tissue classification with bias field inhomogeneity correction to improve the tumor probability map.

C. Initialization

Many conventional snakes require the user to initialize the snake with a bubble either completely inside or completely outside the object to be segmented. The competition snake does not have any constant-velocity inward/outward propogation force, so it can be initialized with some parts of the contour inside and some parts outside the object to be segmented. The competition snake is more robust to variable initialization. We choose the level 0 set of the tumor probability map, where P(tumor)=P(non-tumor), as the initialization. The implicit function is initialized to the distance map of the initial contour, as shown in Figure 3(b). In this way we have an automatic initialization of the snake; the user is not required to define seed points or bubbles completely inside the object to be segmented.

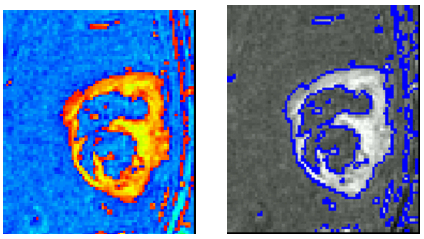

(a) (b)

Fig. 3. (a) Probability map of tumor vs. non-tumor. Voxels tentatively classified as tumor are in orange; voxels classified as non-tumor are in blue. (b) Initialization of the snake.

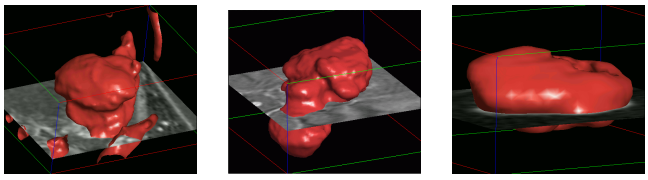

(a) (b) (c)

Fig. 5. Final segmentations (300 iterations) of other tumor datasets. (a) Tumor022, (b) Tumor025, (c) Tumor026.

D. Level set evolution

Figure 4 shows the implicit function ϕ and the level-set snake at several stages in the segmentation of one tumor dataset. The initialization of the snake corresponds to a simple intensity windowing of the image dataset and shows the difficulty of segmenting tumors with the standard erosion-connectivity-dilation morphological operators. After 20 iterations the snake segmentation is essentially complete; the small blobs in the perimeter artifacts of the edge of the bounding box, and are easily removed by eliminating all but the largest connected component.

Also shown is the snake after 300 iterations: the balancing force $P(A) - P(B)$ makes the snake very stable; it does not leak into neighboring structures. Classical snakes that use the gradient magnitude as image force often have difficulty when the boundary of the object to be segmented has gaps with weak step edges in the image; they have a tendency to leak through these gaps when pushed by a constant-sign propagation force.

E. Validation

The level-set procedure was successfully run on several tumor datasets, and compared with hand segmentation by an in-house expert rater. The output of each segmentation is a binary image on the same voxel grid as the original MRI. We used the VALMET [11] image segmentation validation framework to examine various metrics of agreement

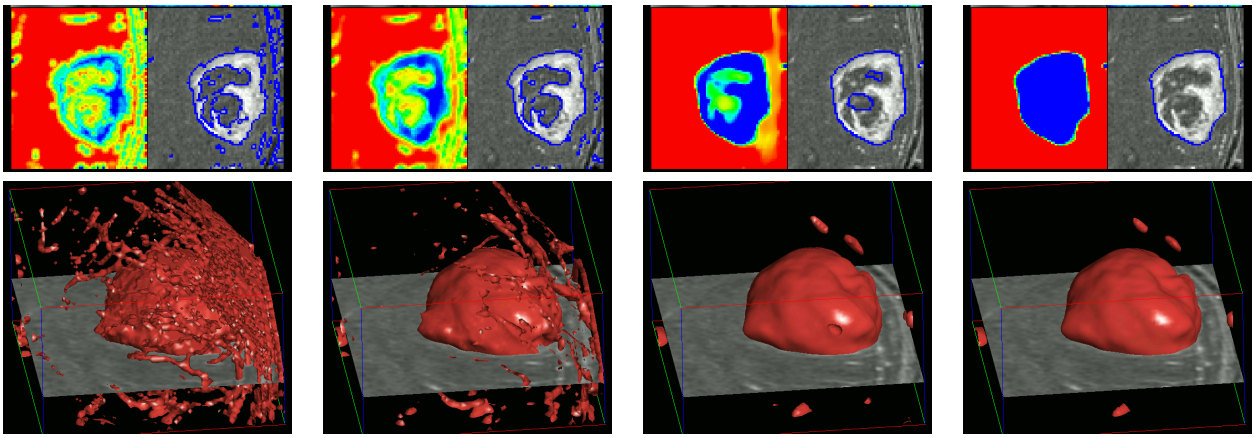

(a) (b) (c) (d)

Fig. 4. A slice through the implicit function (top) and the level-set snake (bottom) for dataset Tumor020, at (a) initialization, (b) 1 iteration, (c) 20 iterations, and (d) 300 iterations. $c_{\mathrm{MCF}} = 0.7$, $\alpha = 3$, and $c_{\mathrm{sm}} = 0.45$

of segmentation. The results for three tumor datasets are shown in Figure 6. The volume overlap measure is a normalized count of voxels in the intersection of two segmentations X and Y, given by $(X \cap Y)/(X \cup Y)$. The Hausdorff distance from X to Y is $max_{x \in X} dist(x, Y)$. Since this is not symmetric, the symmetric Hausdorff metric is the larger of Haus(X,Y) and Haus(Y,X). We also calculate the average distance inside or outside from a point on one surface to the closest point on the other surface.

Dataset	overlap	Haus.	in	out	avg
Tumor020	93.2%	6.92	0.47	1.07	0.59
Tumor022	89.5%	13.02	0.49	4.13	1.49
Tumor025	84.7%	10.73	0.83	1.07	0.85

Fig. 6. Comparison of automatic segmentation with manual segmentation. Surface distances are in voxels.

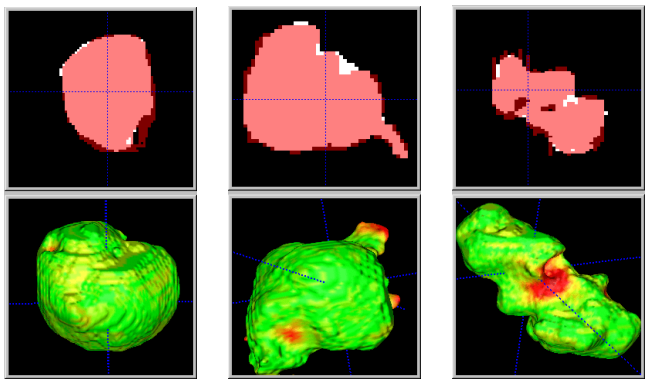

(a) (b) (c)

Fig. 7. Comparison of automatic procedure with manual segmentation. Top: 2D slice: snake in white, manual in red. Bottom: surface distance, -4 (red) to +4 (blue) voxels. Green is within ±2 voxels. Datasets: (a) Tumor020, (b) Tumor022, (c) Tumor025.

V. Discussion

We demonstrate a stable, 3D level-set evolution framework applied to automatic segmentation of large blobby-shaped brain tumors in MRIs, using a probability map of tumor versus background to guide the snake propagation. A nonlinear fit of a mixture model to the histogram provides a fuzzy classification map of gadolinium-enhancing voxels, and this probability map is used to guide the propagation of the snake. The snake is very stable, converging in 20-50 iterations and remaining at its solution without "leaking". The snake is also robust to initialization: in the segmentation results shown here, we use an automatic initialization at the $P(A) = P(B)$ boundary between tumor and non-tumor regions. However, preliminary tests with various initializations indicate the snake can grow into the entire tumor even when the initalization covers only a small portion of the tumor. Preliminary comparisons demonstrate that the automatic segmentation comes close to the manual expert segmentation. Currently, we are validating the machine segmentation versus repeated segmentations provided by several experts. We are also investigating the sensitivity towards initialization and parameter settings on a larger set of tumor datasets.

References

[1] M. Kass, A. Witkin, and D. Terzopoulos, "Snakes: Active shape models," *International Journal of Computer Vision*, vol. 1, pp. 321–331, 1987.

[2] H. Tek and B.B. Kimia, "Image segmentation by reaction-diffusion bubbles," in *International Conference on Computer Vision (ICCV'95)*, 1995, pp. 156–162.

[3] H. Tek and B.B. Kimia, "Volumetric segmentation of medical images by three-dimensional bubbles," *Computer Vision and Image Understanding (CVIU)*, vol. 65, no. 2, pp. 246–258, 1997.

[4] R. Goldenberg, R. Kimmel, E. Rivlin, and M. Rudzsky, "Fast geodesic active contours," in *Scale-Space Theories in Computer Vision*, 1999, pp. 34–45.

[5] M. Leventon, E. Grimson, and O. Faugeras, "Statistical shape influence in geodesic active contours," in *Proc. IEEE Conference Computer Vision and Pattern Recognition (CVPR)*, 2000.

[6] S. Zhu and A. Yuille, "Region competition: Unifying snakes, region growing, and Bayes/MDL for multi-band image segmentation," in *International Conference on Computer Vision (ICCV'95)*, 1995, pp. 416–423.

[7] S. Warfield, J. Dengler, J. Zaers, C.R.G. Guttman, W.M. Wells, G.J. Ettinger, J. Hiller, and R. Kikinis, "Automatic identification of gray matter structures from MRI to improve the segmentation of white matter lesions," *Medical Image Computer and Computer-Assisted Intervention (MICCAI'96)*, vol. 1, no. 6, pp. 326–338, 1996.

[8] S. Warfield, M. Kaus, F.A. Jolesz, and R. Kikinis, "Adaptive template moderated spatially varying statistical classification," in *Medical Image Computer and Computer-Assisted Intervention (MICCAI'98)*, William M. Wells, Alan Colchester, and Scott Delp, Eds. Oct 1998, vol. 1496 of *Lecture Notes in Computer Science*, Springer.

[9] M.R. Kaus, S.K. Warfield, A. Nabavi, E. Chatzidakis, P.M. Black, Jolesz F.A., and Kikinis R., "Segmentation of meningiomas and low grade gliomas in MRI," in *Medical Image Computer and Computer-Assisted Intervention (MICCAI'99)*, Chris Taylor and Alan Colchester, Eds. Sept 1999, vol. 1679 of *Lecture Notes in Computer Science*, pp. 1–10, Springer.

[10] F. Maes, A. Collignon, D. Vandermeulen, G. Marchal, and P. Suetens, "Multi-modality image registration by maximization of mutual information," *IEEE Transactions on Medical Imaging*, vol. 16, no. 2, pp. 187–198, Apr 1997.

[11] G. Gerig, M. Jomier, and M. Chakos, "VALMET: a new validation tool for assessing and improving 3D object segmentation," in *Medical Image Computing and Computer-Assisted Intervention (MICCAI'01)*, W Niessen and M Viergever, Eds., New York, Oct 2001, vol. 2208, pp. 516–523, Springer.